

Scratch that! An Evolution-based Adversarial Attack against Neural Networks

Malhar Jere

University of California San Diego

Loris Rossi*

Politecnico di Milano

Briland Hitaj

SRI International

Gabriela Ciocarlie

SRI International

Giacomo Boracchi

Politecnico di Milano

Farinaz Koushanfar

University of California San Diego

Abstract

We study black-box adversarial attacks for image classifiers in a constrained threat model, where adversaries can only modify a small fraction of pixels in the form of scratches on an image. We show that it is possible for adversaries to generate localized *adversarial scratches* that cover less than 5% of the pixels in an image and achieve targeted success rates of 98.77% and 97.20% on ImageNet and CIFAR-10 trained ResNet-50 models, respectively. We demonstrate that our scratches are effective under diverse shapes, such as straight lines or parabolic Bézier curves, with single or multiple colors. In an extreme condition, in which our scratches are a single color, we obtain a targeted attack success rate of 66% on CIFAR-10 with an order of magnitude fewer queries than comparable attacks. We successfully launch our attack against Microsoft’s Cognitive Services Image Captioning API and propose various mitigation strategies.

1 Introduction

Deep Neural Networks (DNNs) have achieved state-of-the-art results in image classification [24, 25, 29, 46, 48], machine translation [16, 17, 39], and reinforcement learning tasks [6, 44, 45, 51], and have been adopted for a wide array of tasks, such as cancer detection [1, 42], malware detection [30, 40, 50], speech recognition [22], and more. However, despite these accomplishments, DNNs are surprisingly susceptible to deception by adversarial samples [49], which consist of images containing sub-perceptual noise, invisible to humans, that can lead a neural network to misclassify a given input. The adversarial samples can be: (1) targeted (i.e., the goal is to make the model classify the samples to an adversarially desired outcome), or (2) untargeted (i.e., the misclassification can be attributed to any class that is not the ground truth). Researchers have demonstrated that adversarial samples that transfer to the real-world can be printed on



(a) Original Image.



(b) Adversarial Image

Figure 1: Adversarial attack on Microsoft’s Cognitive Services Image Captioning API. Generated caption for Image 1a: ‘*a large passenger jet flying through a cloudy blue sky*’. Generated caption for Image 1b: ‘*a group of people flying kites in the sky*’. Best viewed in color.¹

paper or 3D-models [5], and can target classifiers in different domains, such as images [49], speech [12], and text [3].

The majority of existing adversarial sample-generation techniques for image classifiers focuses on invisible perturbations that often cover the entire image, where the maximum perturbation added to the image is upper bounded according to an L_p -norm metric. These include the L_0 norm [38], which captures the number of perturbed image pixels; the L_1 [13, 36] norm, which measures the Manhattan norm or absolute sum of perturbation values; the L_2 norm [10], which measures the Euclidean distance of the perturbation; or the L_∞ norm [19, 32], which is the largest perturbed value.

In most of these threat models, the adversary has white-box access to the model parameters, i.e., the adversary has full knowledge of the model parameters and training data. Consequently, in these cases, the adversary can easily calculate gradients with respect to the inputs. While these attacks exemplify the significant risks to which neural networks might be exposed, they often do not reflect a realistic threat scenario against computer vision models deployed in the real world, which is often a black-box scenario, where adversaries have

*Work done when the author was a Visiting Graduate Student at University of California San Diego

¹An anonymized video demonstration of the attack can be found here: <https://www.youtube.com/watch?v=WminC14RLey>

limited queries and no access to the model architecture or parameters.

This paper proposes a new parametric L_0 black-box adversarial attack against machine learning (ML) models for this limited, but realistic threat scenario. In the threat model, the adversary can only modify pixels in a constrained manner. We call these modifications adversarial scratches, inspired by the scratches commonly found in actual printed images. Our scratches are parametrized as simple geometric shapes: line segments or second-degree Bézier curves, which are evolved through Evolution Strategies, as highlighted in Figure 2. We furthermore enforce a query budget to simulate rate limiting for real-world ML systems.

We propose two novel evolutionary black-box neural network attacks, for which the only available information is the confidence for an image caption or for individual class labels.

1.1 Contributions

- *Adversarial scratches*, a new class of constrained black-box attacks for image classifiers. Adversarial scratches leverage Evolution Strategies, where scratches are evolved parametrically according to a pre-defined fitness function, and can successfully attack ResNet-50, VGG-19, and AlexNet architectures trained on the CIFAR-10 and ImageNet datasets.
- *Attack effectiveness evaluation* across a variety of attack parameters, including query dependence, scratch shape, scratch location, and scratch color. Even in the extremely constrained case with a single color for a single scratch, our attacks achieved a 66% targeted success rate for CIFAR-10 trained neural networks.
- *Successful attack deployments* in both image and network domains, similar to LaVAN work by Karmon et al. [27]. The image-domain scratches are restricted to lie within the normal dynamic image range of $[0, 1]$; the network-domain scratches are not necessarily restricted on predefined bounds.
- A *real-world attack* against Microsoft’s commercially available Cognitive Services Image Captioning API. Our attacks successfully fooled the API into producing wrong captions or no captions (an example of a successful attack is demonstrated in Figure 1), thereby demonstrating a real-world manifestation of an adversarial attack on ML systems. We have contacted Microsoft regarding this vulnerability.
- *Countermeasures* to our attacks. We propose, evaluate, and discuss different countermeasures to our attacks including, JPEG compression, median filtering, and image clipping, and we assess their effectiveness in mitigating the effect of adversarial scratches and their impact on benign images.

1.2 Organization

The rest of the paper is organized as follows: In Section 2, we discuss related work and provide the necessary background information. Section 3 discusses the methodology pursued to generate adversarial scratches. Section 4 and Section 5 depict our experimental setting and our results, respectively. In Section 6, we further elaborate on our results, initial failed attempts, and potential defense strategies. We provide our conclusions and future directions in Section 7.

2 Background and Related Work

There is extensive prior work on generating adversarial samples for neural networks across multiple input domains. We highlight the different types of adversarial attacks on neural networks and provide a quick overview of the evolution strategies used in our work.

2.1 Adversarial Attacks on Neural Networks

Prior works on adversarial attacks on neural networks consist of methods to deceive [4, 10, 19, 38] or cause denial-of-service of neural networks [43]. Our work considers adversarial attacks that attempt to deceive image classifiers. We consider a neural network $f(\cdot)$ used for classification where $f(x)_i$ represents the softmax probability that image x corresponds to class i . Images are represented as $x \in [0, 1]^{w.h.c}$, where w, h, c are the width, height, and number of channels of the image. We denote the classification of the network as $C(x) = \arg \max_i f(x)_i$, with $C^*(x)$ representing the ground truth of the image. Given an image x and an adversarial sample x' , the adversarial sample has the following properties:

- $L(x' - x)$ is small for some image distance metric L .
- $C(x') \neq C^*(x) = C(x)$. This means that the prediction on the adversarial sample is incorrect whereas the original prediction is correct.

Biggio et al. [8] were the first to show the occurrence of adversarial examples in Support Vector Machines, while Szegedy et al. [49] discovered that deep neural networks are prone to such attacks as well. Since then, there has been a plethora of works generating adversarial samples for both white and black-box scenarios.

White-Box Adversarial Attacks. In the white-box threat scenario, adversaries have full access to the neural network parameters and can calculate gradients with respect to inputs. Most white-box adversarial sample attacks characterize robustness with respect to the L_p norm, as outlined below.

- **L_0 -norm** attacks limit the number of perturbed pixels. Several examples include the JSMA attack [38], which finds vulnerable pixels through saliency maps for inputs,

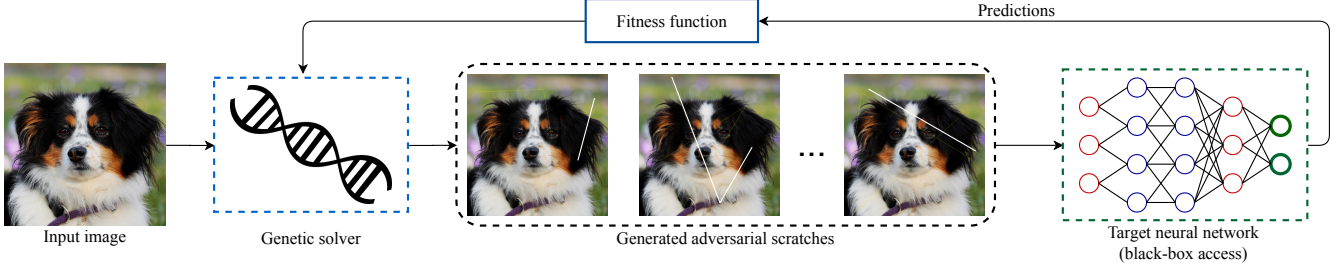


Figure 2: Framework to generate variable location adversarial scratches. Scratch parameters include: (1) number of scratches, (2) domain of scratches (image or network domain), (3) location parameters of scratch (fixed or variable), (4) population size, (5) number of iterations, (6) mutation and crossover rate. Best viewed in color.

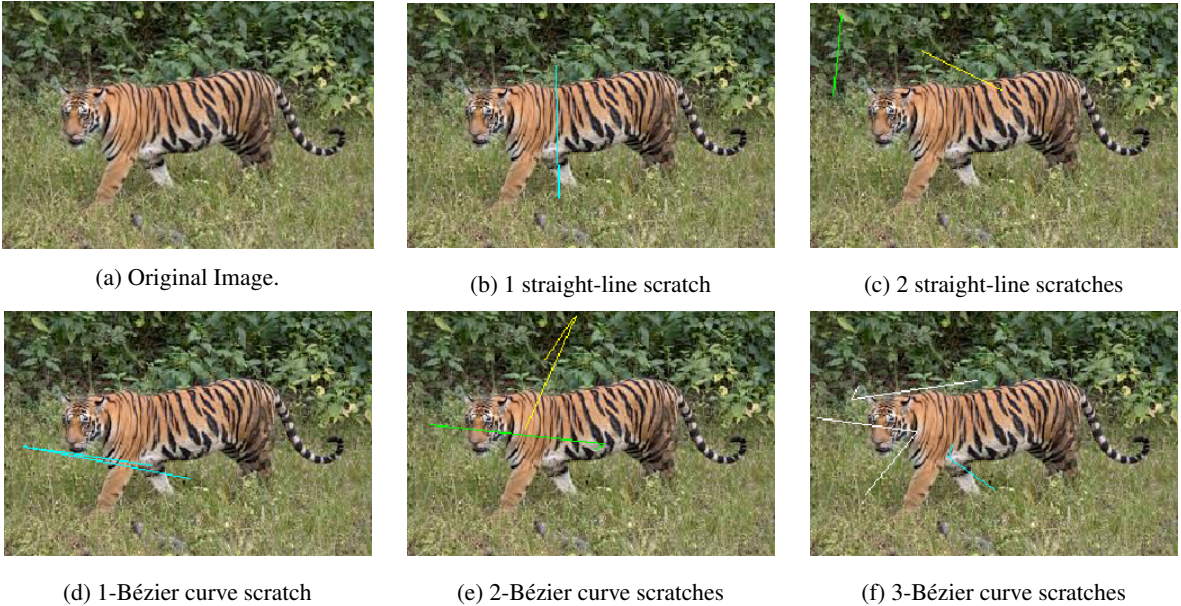


Figure 3: Adversarial Scratches can have diverse manifestations, such as Bézier Curves or Straight Lines. Individual scratches for the same image may have different colors. Best viewed in color.

SparseFool [35], which exploits the low mean curvature of decision boundaries, and [37], which uses greedy search to find adversarial perturbations.

- **L_1 -norm** attacks place an upper bound on the Manhattan distance or absolute sum of perturbation values. Examples include DeepFool [36] and the EAD attack [41].
- **L_2 -norm** attacks place an upper bound on the Euclidean distance of the adversarial perturbation. A notable example is the Carlini-Wagner L2 [11] attack, which performs gradient descent on the predicted perturbation norm.
- **L_∞ -norm** attacks place an upper bound on the maximum perturbation that can be applied to each pixel. Notable examples include the Fast Gradient Sign Method [19] and the Projected Gradient Descent method [32].

In addition to L_p -norm constrained attacks, several other

attacks use gradient information, such as LaVAN [27] and adversarial patches [9].

Black-box Adversarial Attacks. In the black-box threat scenarios adversaries possess limited information of the parameters of the neural network under attack. This threat model may range from adversaries having access to the full prediction vector, i.e., *soft-label*, to simply having access to the top predicted label, i.e., *hard-label*. Black-box attacks are generally more challenging to implement than their white-box counterparts due to limited information available to the adversary.

Recent literature has proposed numerous black-box attacks that restrict perturbations with respect to an L_2 or L_∞ norm constraint. Narodytska and Kasiviswanathan [37] use a naive policy of perturbing random segments of an image to generate adversarial examples. Bhagoji et al. [7] reduce the feature space dimensions using PCA and random feature grouping before estimating gradients. Chen et al. [14] use finite differ-

ences to estimate gradients for a gradient based-attack. Ilyas et al. [26] use Natural Evolutionary Strategies to estimate gradients, while GenAttack [2] uses genetic algorithms to estimate gradients. Guo et al. [20] identify that low-frequency perturbations allow for improved query efficiency for black-box attacks, which is further evaluated in SimBA [21]. Lin et al. utilize differential evolution to generate L_2 -norm bounded adversarial perturbations [31].

In contrast to these works, L_0 -norm bounded black-box attacks are rarely explored. The One-Pixel Attack [47] uses Differential Evolution to find the optimal (x, y) pixel coordinates and RGB values, but it has a poor success rate on larger neural networks and requires several thousand queries. The PatchAttack [52] method uses reinforcement learning to optimally place pre-generated textured patches, however, the patches are often very large and highly visible, covering up to 20% of the entire image. The Adversarial scratches discussed in our work use Differential Evolution, similar to the One-Pixel Attack, but proposes a parametric model for the perturbation which vastly reduces the number of search parameters. Finally, our approach implements a physical attack on a real-world image classification framework.

2.2 Evolution Strategies

The generation of adversarial scratches uses evolution strategies, which are population-based gradient-free optimization strategies. They are roughly inspired by the process of natural selection, in which a population P of candidate solutions is generated at each iteration, termed a *generation*. Candidate solutions are evaluated using a *fitness function*, and "fitter" solutions are more likely to be selected to breed the next generation of solutions. The whole process terminates either when a candidate solution satisfies some pre-defined criteria, or when the maximum number of generations is reached. The next generation is generated through a combination of *crossover* and *mutation*. Crossover involves taking numerous parent solutions, combining their parameters, and generating a new generation of solutions, similar to biological reproduction. Mutation applies small random perturbations to population members to increase the diversity of population members and provide a better exploration of the search space. Evolution strategies are particularly suited for black-box optimization, as they do not require any information about the underlying fitness function. Our work uses the Differential Evolution (DE) and Covariance-Matrix Adaptation Evolution Strategies (CMA-ES) algorithms.

Differential Evolution. Differential Evolution is an evolution strategy that allows for constrained optimization of algorithm parameters within a certain bound. This is highly advantageous for generating adversarial scratches for real-world scenarios where perturbations are restricted to be in the dynamic range of images. Algorithm 1 highlights the steps to generate potential candidates for a given set of parameters to

Algorithm 1: Differential Evolution for a fitness function F , which draws the adversarial scratch and evaluates the model performance on the scratched image. The algorithm parameters are population size λ , number of iterations N , mutation rate m , cross-over rate CR , and bounds for each candidate solution $BOUNDS$. It returns candidate $x \in \mathbb{R}^n$, where n is the size of the solution vector being evaluated.

```

Require:  $F, \lambda, N, m, CR, BOUNDS$ 
 $X \leftarrow uniform\_random\_generator(\lambda, n, [0, 1])$ 
for  $i = 1$  to  $N$  do
    for  $j = 1$  to  $\lambda$  do
         $x = X_j$ 
         $p, q, r \leftarrow random\_sample(3, n)$ 
         $s.tp \neq q \neq r$ 
         $a, b, c \leftarrow X[p, q, r]$ 
         $MUTANT = clip(a + m \times (b - c), BOUNDS)$ 
         $r = uniform\_random\_generator(n, [0, 1])$ 
        for  $k = 1$  to  $n$  do
            if  $r_k \leq CR$  then
                 $y_k = MUTANT[k]$ 
            else
                 $y_k = x[k]$ 
            end if
        end for
        if  $F(y) \leq F(x)$  then
             $X_j = y$ 
        end if
    end for
end for
return  $x \in X$  such that  $F(x) < F(x_k) \forall k \in \{1, 2, \dots, N\}$ 

```

the Differential Evolution solver.

CMA-ES. Covariance Matrix Adaptation Evolution Strategy (CMA-ES) is an evolution strategy used for the optimization of real non-convex functions in a continuous domain and it is considered a state-of-the-art algorithm in evolutionary computation [23]. At each generation, CMA-ES samples a population of candidate solutions from a multivariate normal distribution, whose mean, standard deviation, and covariance matrix are updated after each iteration. The covariance matrix is used to track pair-wise dependencies of the optimized parameters; this allows the solver to dynamically change the degree of exploration during the optimization process. Algorithm 2 shows how CMA-ES works on a high level, with covariance matrix C , and evolution paths p_c and p_σ . For further details on its implementation, please refer to the CMA-ES author's tutorial [23].

3 Methodology

In this section we frame the generation of adversarial scratches as a constrained-optimization problem. We highlight the parameters used to generate scratches as well as

Algorithm 2: Covariance Matrix Adaptation Evolution Strategy for a fitness function F . The algorithm parameters are population size λ , number of iterations N , mean vector $\mu \in \mathbb{R}^n$, and step size σ_k , where n is the size of the solution vector being evaluated. It returns candidate $x_1 \in \mathbb{R}^n$ or μ

```

Require:  $F, \lambda, N, \mu, \sigma_k$ 
    {Initialize variables}
     $C = I, p_\sigma = 0, p_c = 0$ 
    for  $i = 1$  to  $N$  do
        {Generate new population}
        for  $j = 1$  to  $\lambda$  do
             $x_j = \text{sample\_from\_N}(\mu, \sigma^2 C)$ 
             $f_j = F(x_j)$ 
        end for
        {Sort best candidates and update all parameters}
         $x_{1\dots\lambda} = x_{s(1)\dots s(\lambda)}$  with  $s(i) = \text{argsort}(f_{1\dots\lambda}, j)$ 
         $\mu' = \mu$ 
         $\mu \leftarrow \text{update\_means}(x_1, \dots, x_n)$ 
         $p_\sigma = \text{update\_ps}(p_\sigma, \sigma^{-1} C^{-1/2} (\mu - \mu'))$ 
         $p_c = \text{update\_pc}(p_c, \sigma^{-1} (\mu - \mu'), \|p_\sigma\|)$ 
         $C = \text{update\_c}(C, p_c, (x_1 - \mu')/\sigma, \dots, (x_\lambda - \mu')/\sigma)$ 
         $\sigma = \text{update\_sigma}(\sigma, \|p_\sigma\|)$ 
    end for
    return  $x_1$  or  $\mu$ 

```

characterize scratch generation techniques depending on the dynamic range of images.

3.1 Problem Description

Formally, we consider an image classifier f represented as $f : [0, 1]^{w.h.c} \rightarrow \mathbb{R}^K$ where K is defined as the number of classes. $f(x)_i$ represents the softmax probability that input x corresponds to class i . Images are represented as $x \in [0, 1]^{w.h.c}$, where w, h, c are the width, height, and number of channels of the image. The goal of the adversary is to produce an adversarial sample $x' \in [0, 1]^{w.h.c}$ that satisfies the following properties:

$$\begin{aligned} & \text{maximize } f(x')_{\text{adversarial}} \\ & \text{subject to } L(x' - x) \leq d \end{aligned}$$

Here $L(\cdot)$ represents some distance metric for the adversarial perturbation, which is often minimized or upper-bounded. Prior works often involved utilizing the L_p norm as the distance metric. In this vein, our work is most similar to L_0 -norm bounded attacks.

3.2 Proposed Solution

We propose the first parametric black-box L_0 attack where the adversarial perturbations are added in the form of scratches

on an image. In particular a perturbation $\delta \in \mathbb{R}^{w.h.c}$ is confined over a small area of the image x defined by the support of the scratch, the scratch mask $m \in \{0, 1\}^{w.h}$. Scratches are defined as

$$x' = (1 - m) \odot x + m \odot \delta, \quad (1)$$

where \odot denotes the element-wise multiplication.

Scratches can be manifested either as Bézier curves [18] or as line segments, and can consist of a single color for all pixels belonging to a scratch or have distinct colors for each pixel. Ours is the first attack to adopt a parametric model to define the scratch mask m , which is key to reducing the number of attack parameters. Adversarial scratches often look like natural artifacts but can significantly affect the prediction of neural networks. Parametric modeling of the scratches allows for flexible attacks on an image.

Depending on the attack scenario, we choose to keep the mask m fixed or to evolve its parameters via Differential Evolution. We divide our attacks into two setups based on the real-world feasibility of the attack, namely the *image domain* and the *network domain*. In the image domain, the scratch values are restricted to lie in the dynamic range of images; that is, the pixel values of the adversarially scratched image x' values must lie in the range $[0, 1]$ for RGB images. We initially attempted to keep the mask m fixed but found that this method would often get stuck in local minima, following which we chose to evolve m via Differential Evolution. The network domain imposes no such restrictions on the scratches and the adversarial scratch values can exceed the image range.

We generate image-domain scratches through Differential Evolution due to its ability to specify input constraints such as scratch location and pixel values. We obtain network-domain scratches through the CMA-ES algorithm due to its ability to find solutions effectively in an unconstrained search space and through Differential Evolution by relaxing the constraints on the dynamic range of pixel values.

3.3 Image-Domain Attack

In the image-domain attack, individual scratches are evolved according to Differential Evolution. Our initial attempts to generate scratches with fixed scratch locations were unsuccessful. These experiments are described in-depth in Section 6.

Each scratch in the image-domain can be represented as line segment or as a second-order rational Bézier curve [53], which is a parametric curve commonly used in computer graphics and robotics. A Bézier curve uses 3 anchor points $P_0 = (x_0, y_0)$, $P_1 = (x_1, y_1)$ and $P_2 = (x_2, y_2)$ with a weighting coefficient W to draw a curve according to the following equation:

$$B(t) = \frac{(1-t)^2 P_0 + 2(1-t)tWP_1 + t^2 P_2}{(1-t)^2 + 2(1-t)tW + t^2} \quad (2)$$

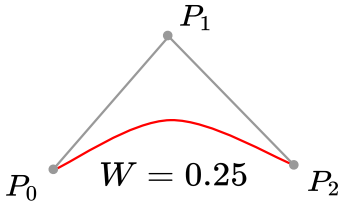


Figure 4: Second-degree Bézier curve with anchor points and weighting coefficient used to generate scratches.

For image-domain attacks, the perturbation parameters are encoded into an array, which is also termed the candidate solution. For single-scratch Bézier curve attacks, the candidate solution is a 10-dimensional vector consisting of the following:

- $(x_0, y_0), (x_1, y_1), (x_2, y_2)$ for P_0, P_1 , and P_2 respectively, namely the x-y coordinates for the anchor points. Each (x, y) pair is constrained to be between $[0, w], [0, h]$ so as to be within the image dimensions.
- W , the weighting coefficient used to control the shape of the curve. Constrained between $[0, 7]$.
- R, G, B consisting of the pixel values for each of the color channels of the adversarial scratch δ . For image domains, they are constrained between $[0, 1]$.

For line segments, the scratches are encoded as a 7-dimensional vector consisting of the following:

- $(x_0, y_0), (x_1, y_1)$ for P_0 and P_1 , the x-y coordinates for the starting and ending points of the line segment. Each (x, y) pair is constrained between $[0, w], [0, c]$.
- R, G, B consisting of the pixel values for each of the color channels of the adversarial scratch δ . For image domains, they are constrained between $[0, 1]$.

Multiple scratches consist of copies of the same set of variables encoded in the same array. For example, an array for 2 Bézier curve scratches would be 20-dimensional, with the first 10 devoted to the first scratch and the next 10 devoted to the second scratch.

Fitness Function. We outline the algorithm to generate targeted attacks as follows. Formally, let $F : \mathbb{R}^d \rightarrow \mathbb{R}$ be the fitness function that must be minimized for differential evolution, with the image classifier f represented as $f : [0, 1]^{w.h.c} \rightarrow \mathbb{R}^K$. The fitness function takes in the candidate solution as a vector of real numbers and produces a real number as output, which indicates the fitness of the given candidate solution. A reasonable expectation for the fitness function is to directly

use the target class softmax probability; however, we observed that it is more efficient and effective to jointly minimize the top class, while attempting to maximize the target class probabilities, in addition to using their logarithms for numerical stability. Specifically, for a target class t with source class s , we maximize the following to steer the network output towards class t :

$$F(x) = \alpha \times \log(f(x)_t) - \beta \times \log(f(x)_s), \quad (3)$$

After performing a grid search, we observe that the parameters $\alpha = 1, \beta = 50$ offer the best attack success rate. To generate the adversarial sample x' , we used this fitness function in an iterative manner. This fitness function was then used to evaluate candidates at each generation in Algorithm 1.

For untargeted attacks, we modify the fitness function as follows:

$$F(x) = - \sum_{i=0}^K f(x)_i \times \log(f(x)_i) \quad (4)$$

as this would maximize the entropy of the classifier predictions rather than the prediction on any particular class.

3.4 Network-Domain Attack

Network-domain attacks may be evolved according to Differential Evolution or CMA-ES, and may be further divided into two types depending on whether the parameters that govern the scratch locations are fixed or variable. Unlike fixed-scratch attacks in the image domain, we were able to obtain successful results for this setting. We explore two options that control the locations for each scratch.

Fixed Scratch Location. In the network-domain attack, scratches are either represented as a line segment parametrized by starting and ending points $P_0 = (x_0, y_0)$ and $P_1 = (x_1, y_1)$, or as a second-order Bézier curve with points $P_0 = (x_0, y_0), P_1 = (x_1, y_1)$, and $P_2 = (x_2, y_2)$ with a weighting factor W , similar to the image-domain scenario. We randomly choose a mask m that stays fixed throughout the attack, and evolve the value of each pixel belonging in the scratch rather than assigning a single color to each scratch as in the image-domain attacks. Thus, for a scratch covering M pixels on a RGB image, the adversarial scratch values can be written as a vector with $3M$ elements. This leads to a much larger search space for which we use the Covariance Matrix Adaptation Evolutionary Strategy (CMA-ES). We settled upon CMA-ES due to its ability to find solutions in larger and unconstrained environments, which make it suitable for network-domain attacks. We utilized the same fitness function used for the Image Domain.

Variable Scratch Location. In the variable scratch location, we repeated the experiments of the image-domain experiment, but relaxed the constraint on the pixel value range, allowing it to have any value, rather than being restricted to $[0, 1]$.

4 Experimental Setup

We describe the experimental setup for our scratches on the ResNet-50 and VGG-16 neural networks trained on CIFAR-10 and pre-trained ImageNet ResNet-50 and AlexNet networks, considering both image-domain and network-domain attacks.

4.1 Image-Domain Setup

We trained ResNet-50 [24] and VGG-16 [46] models on the CIFAR-10 [28] dataset and achieved test accuracies of 93.91% and 85.77%, respectively. In addition to attacking these models for CIFAR-10, we attacked ImageNet pre-trained AlexNet [29] and ResNet-50 models. All attacks were performed on correctly classified images.

For CIFAR-10 targeted attacks, we utilized the fitness function outlined in Equation 3. We observed that CIFAR-10 attacks are most effective with a population size of 50, mutation rate 0.8, 50 iterations, and cross-over rate 0.7. We observed that targeted attacks on ImageNet trained models failed to converge after several hundred iterations; hence, we proceeded with the untargeted fitness function, outlined in Equation 4, with a population size of 100 over 100 iterations, based on a grid search on potential populations and iterations. All CIFAR-10 experiments were conducted on 1000 test-set images, and ImageNet experiments were conducted on 100 validation set images.

4.2 Network Domain Setup

Fixed Scratch Location. We conducted our network-domain experiments on the ResNet50 model [24], with testset accuracy of 93.91% and 76.13% (top-1 accuracy) for CIFAR10 and ImageNet, respectively. All the attacks were performed on 100 images for ImageNet and 1000 for CIFAR-10 taken from the validation set. Selected images were originally correctly classified by the model.

Each image evaluation involved a different number of adversarial scratches whose pixel values were optimized with the CMA-ES algorithm. The algorithm was initialized with parameters $\mu = 0$ and $\sigma = 0.5$, and a population size $\lambda = 40$, chosen after hyperparameter tuning (described in Section 5.2). For CIFAR-10 and ImageNet attacks, the maximum number of iterations were set to 40 and 400, respectively, for a total of 16,000 and 160,000 maximum queries, respectively.

All network-domain attacks were targeted. Targets were chosen at random and were fixed for each source image to make fair comparisons between attacks on the same image with different numbers of scratches. To reduce the effects of lucky initialization of the location of the scratches, each image was attacked 10 times with different random scratches locations chosen each time.

5 Results

We evaluated our scratches on the ResNet-50 and VGG-16 neural networks trained on CIFAR-10 and pre-trained ImageNet ResNet-50 and AlexNet networks. For each dataset, we evaluated both image-domain and network-domain attacks across different types and numbers of scratches.

5.1 Image Domain

Straight Lines. We first applied adversarial scratches in the form of a straight line, with several examples being demonstrated in Figure 3. Table 1 reports the CIFAR-10 attack success rates. We note that straight line image-domain attacks were less successful on ImageNet, with 2-straight line scratches achieving a 60% success rate.

Bézier Curves. Image-domain attacks demonstrated a high success rate across targeted attacks in CIFAR-10 and untargeted attacks in ImageNet, across Bézier curve and straight line shapes, and across varying numbers of scratches. We observe in Table 1 that more scratches resulted in higher attack success rates, queries were largely independent of the number of scratches, and Bézier-curve-based attacks were more successful than straight-line-based attacks. For ImageNet-based models, we achieved a 70% success rate for 2-Bézier curve attacks with a population size of 500 evaluated over 100 iterations, and 30% success rate for 2 straight lines with the same population and iterations. We observed that image-domain attacks were significantly harder to achieve than network-domain attacks, notably because of the extremely small search space both in terms of dimensionality and the constraints on the upper and lower bounds of the search space. Nevertheless, our experiments show a clear vulnerability in neural-network-based classifiers to this class of attacks. Further details can be found in Table 1.

Comparing to Existing Attacks. We compare our Bézier-curve attack to the one-pixel attack [47], which is the most similar attack. The one-pixel attack uses differential evolution to find *single* pixels that can fool classifiers. For CIFAR-10, we trained a VGG-16 model to a test-accuracy of 85.77%, and compared our single-scratch, image-domain Bézier curve attack to theirs. We obtained an attack success rate of 75.79% for a query limit of 2500 compared to their attack success rate of 5.63% with a query limit of 20,000. Table 3 highlights further dependence on attack cost. For ImageNet-based models, we attacked the AlexNet model and were able to successfully fool 100% of all images under 50,000 queries, while the one-pixel attack achieves a success rate of 16.04% with the same query limit.

Population Size Tuning. To choose an appropriate population size that optimizes for attack success rate as well as latency, we varied the population size and found that a population of 50 offered the best performance.

Physical Attack. We attempted to attack the Microsoft Cogni-

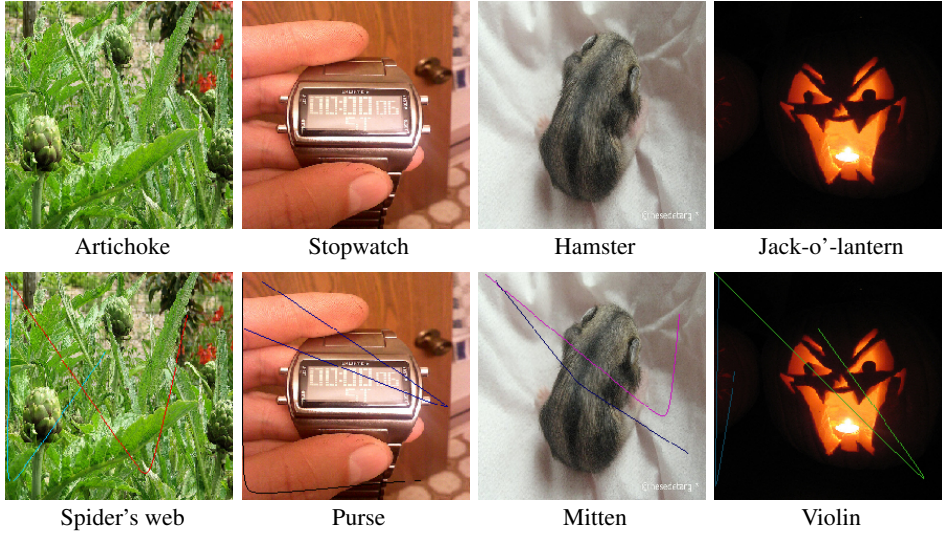


Figure 5: Variable location, double scratch attacks on ImageNet in the image domain. The top row contains the original images and their respective class label. The bottom row images are adversarial samples generated via our double-scratch attack and the predicted class when evaluated on ResNet-50 [24].

Image Domain							
Bézier Curves				Straight Lines			
Scratches	Success Rate	Queries	Coverage	Scratches	Success Rate	Queries	Coverage
1	66.25%	711	4.13%	1	61.1%	456	2.64%
2	86.5%	1140	5.95%	2	75.39%	581	4.96%
3	92.06%	899	7.48%	3	83.33%	490	6.82%

Table 1: Variable-location image-domain scratch attack results for ResNet-50 trained on CIFAR-10. More scratch coverage resulted in higher success rates, with Bézier curves offering a better attack success rate than straight lines.

Image Domain							
Bezier Curves				Straight Line			
Scratches	Success Rate	Queries	Coverage	Scratches	Success Rate	Queries	Coverage
2	70%	30472	0.7%	2	33%	32198	0.56%
3	73%	21988	1.3%	3	42%	25499	0.9%

Table 2: Variable-location image-domain scratch attack results for ResNet-50 trained on ImageNet. More scratch coverage resulted in higher success rates, with Bézier curves offering a better attack success rate than straight lines. ImageNet requires significantly more queries than CIFAR-10 attacks.

	Single Scratch attack			One pixel attack
Query Limit	2500	10000	20000	20000
Success Rate	75.79%	83.7%	84.7%	5.63%
Pixel Coverage	3.78%	3.77%	3.68%	0.1%

Table 3: Our attack compared to one-pixel attack [47] for VGG-16 trained on CIFAR-10.

tive Services Image Captioning API [33] using our proposed methods. The service provides a descriptive caption of the image as well as its confidence. Our goal was to utilize the confidence as our fitness function and attempt to minimize the confidence to make the API generate fake or missing captions. In this setting, we used 3 scratches, with 50 iterations and a population size of 50, with an upper limit of 2500 queries to the API.

We successfully managed to decrease the caption confidence from an initial value of 0.87 down to 0.25, and were able to deceive the API into generating wrong captions. In

one particular case, the API was not able to generate any captions at all. Several examples of these generated scratches are shown in Table 4.

5.2 Fixed-Location Network Domain

Population Size Tuning. To choose a good value for the population size, we performed attacks on a set of 24 images from CIFAR-10, each time picking a population size from $[5, 10, 20, 40, 80, 150]$. We set the population size as 40, which we observed to give the fewest average number of queries to perform a successful attack (Figure 6).

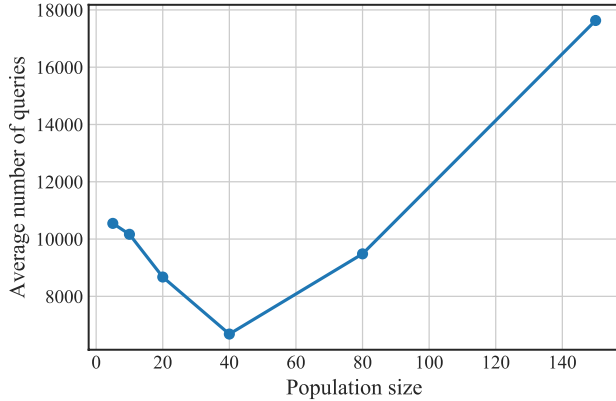


Figure 6: Impact of population size on the average number of queries needed by fixed-location network-domain attacks on CIFAR-10.

Straight lines attacks. Figure 7 shows a few examples of adversarial straight line scratches; Tables 5 and 6 show the results from 100 attacked images. We report the average percentage of pixels covered by successful attacks, the average number of queries of successful attacks, and the success rates. It is evident, particularly in ImageNet results, that using more scratches leads to a lower average number of queries and a higher success rate.

Bézier curves attacks. We changed the shape of the adversarial scratches, this times using quadratic Bézier curves, as explained in Section 3.3. Results are reported in Tables 5 and 6, respectively. We can see again that increasing the number of scratches decreases the number of queries of a successful attack and increases its success rate. Moreover, we can observe that Bézier curves attacks are more effective than the corresponding straight lines attacks, in terms of the number of queries needed and the success rate. Our intuition is that the attacked model uses more information on the shape of the image rather than its colors when making a prediction; hence, a nonlinear scratch like a Bézier curve can better exploit this behavior. This may also explain why a higher number of scratches results in a higher-success rate: scratches located in different parts of an image can exploit more shape-dependent features.

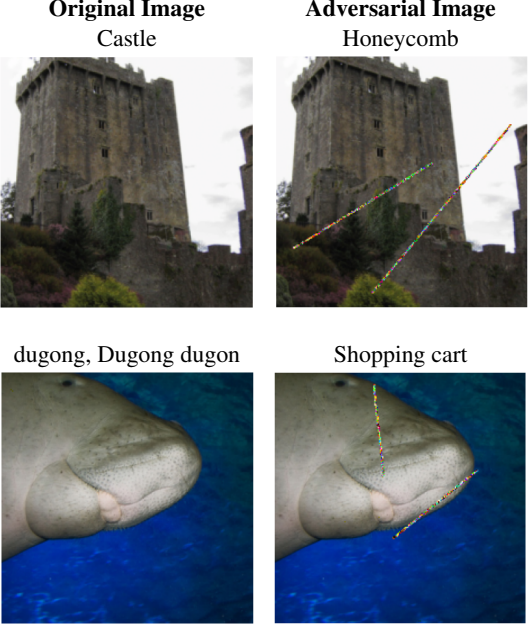


Figure 7: Examples of CMA-ES straight lines attacks in the network domain. Scratches were clipped to the image domain for visualization purposes. The left side shows the original images and their corresponding class; the right side shows the generated adversarial samples (scratches) and their respective predicted labels when evaluated on ResNet-50. Best viewed in color.

5.3 Variable Location Network Domain

Network-domain attacks with variable locations achieve lower success rates than their image-domain counterparts, as illustrated in Table 7. We hypothesize that this may be due to searching over a much larger search space when taking into account the relaxation on the pixel value restrictions. Furthermore, we observe that the majority of variable-location attacks on ImageNet time out with our query budget, motivating the need for a much larger query budget for such attacks.

6 Discussion

6.1 Unsuccessful Image-Domain Scratch Attempts

Prior to obtaining our results, we experimented with a broad range of parameters for the scratches. For the image domain, we attempted the following:

- **CMA-ES.** We initially used CMA-ES with fixed scratch locations and \tanh normalization to implement image-domain attacks similar to the CW attack [11]. However, this yielded an attack success of around 2%, which mo-

Input Image			
Predicted Caption	A large passenger jet flying through a cloudy blue sky	A flock of birds flying in the sky	A group of people flying kites in the sky
Confidence	0.870	0.438	0.406
Input Image			
Predicted Caption	A flock of seagulls flying in the sky	A airplane that is flying in the sky	No caption
Confidence	0.317	0.250	—

Table 4: Successful attacks against the Microsoft Cognitive Services Image Captioning API. The top left image denotes the source image, which is captioned correctly as ‘a large passenger jet flying through a cloudy blue sky’. All other images are examples of images that successfully deceived the captioning service. Best viewed in color.

Network Domain							
Bézier Curves				Straight Lines			
Scratches	Success Rate	Queries	Coverage	Scratches	Success Rate	Queries	Coverage
1	53.80%	31718	0.46%	1	44.00%	34623	0.56%
2	86.40%	25747	0.84%	2	80.50%	30776	0.99%
3	96.70%	16838	1.24%	3	92.40%	23826	1.42%
4	98.77%	11640	1.65%	4	96.40%	18848	1.86%

Table 5: Network domain, fixed-location scratch attack success rate for ResNet-50 trained on ImageNet.

tivated us to use Differential Evolution, which significantly improved attack success rate.

- **Fixed scratch location.** We initially attempted our image-domain attacks with fixed scratch parameters and evolved only the RGB values. This led to our fitness functions often getting stuck in local minima and not converging to the target class; hence, we included the scratch location parameters in the evolution strategy.

6.2 Source-target Dependency in Network Domain

We wanted to analyze whether there was a relationship between the ground truth and the target class with respect to the difficulty of the attack. For practical reasons, we performed the following experiments on CIFAR-10, given that it has

only 10 classes compared to ImageNet with 1000 classes. The results in Figure 9 are based on 500 attacked images with 50 samples per target class. In this figure, rows correspond to source classes, columns correspond to target classes, and cell values correspond to the average number of queries needed to achieve a successful attack.

The mean value for each row, displayed in the right-most column in Figure 9, provides the average number of queries needed to perform a successful attack for images with that particular source class. We observe that not all source classes are equally easy to attack; the deer class is the easiest to attack, while the car and truck classes are the hardest. Conversely, the mean values for each column, displayed in the bottom row of Figure 9, provide the average number of queries required to generate a successful adversarial sample with that class as the target. We observe that not all classes are easy to reach as

Network Domain							
Bézier Curves				Straight Lines			
Scratches	Success Rate	Queries	Coverage	Scratches	Success Rate	Queries	Coverage
1	77.80%	2697	2.97%	1	54.90%	3133	3.28%
2	93.10%	2089	4.21%	2	76.80%	3207	3.96%
3	96.00%	2000	4.54%	3	83.80%	2829	4.30%
4	97.20%	1915	4.69%	4	90.70%	2622	4.40%

Table 6: Network domain, fixed-location scratch attack success rate for ResNet-50 trained on CIFAR-10.

Network Domain							
Bézier Curves				Straight Lines			
Scratches	Success Rate	Queries	Coverage	Scratches	Success Rate	Queries	Coverage
1	52.18%	1578	4.15%	1	63.49%	350	1.98%
2	68.25%	886	6.57%	2	68.45%	410	3.94%
3	75.77%	940	8.62%	3	72.22%	1340	5.1%

Table 7: Network domain, variable-location scratch attack success rate for ResNet-50 trained on CIFAR-10. We use differential evolution with relaxed constraints on the pixel values.

targets; the ship and deer classes require the most queries when chosen as targets.

Furthermore, we attempted to investigate the semantic similarity between source and target classes. We computed word similarity measures using the WordNet dataset [34], with the results highlighted in Figure 10. Given the results in Figure 9, we conjecture that higher similarity between the source and target labels typically results in a more effective attack. For example, for the (truck, car) pair, we need relatively fewer queries to generate targeted attacks towards car classes from a truck image, and vice versa. This phenomena persists for other pairs with similar semantic information, such as (cat, dog) or (bird, plane).

However, we believe that this query dependency is tightly connected with the method used to compute class similarity; for instance, while bird and plane classes share similarity in that they represent flying objects, that is not the case for pairs such as (truck, car) and (dog, cat), as illustrated in Figure 10. One possible conjecture might be that although semantic similarity between classes plays a major role in the ease of an attack, simple tree-based structures such as WordNet are not sufficient. Further work is needed to devise suitable semantic similarity metrics between source and target classes.

6.3 Defenses in Image Domain

Image Filtering. We discuss several possible image filter solutions to prevent image domain adversarial-scratch attacks. We evaluated the following techniques as defenses against adversarial scratched images in the image domain:

- JPEG compression with varying quality factors

- Median filters applied to each channel separately with a kernel size of 3×3 pixels

We capture this behavior through the recovery rate, defined as the fraction of adversarial images that are predicted according to their correct labels after an adversarial scratches attack. Surprisingly, we find that JPEG compression is highly ineffective as a defense against image-domain scratches targeting ImageNet-trained ResNet-50 models. We observe that we recovered 0% of original labels from adversarially scratched images. Correspondingly, JPEG compression also leads to a low recovery rate for CIFAR-10 trained ResNet-50 models. Median filtering offers a better recovery rate, as highlighted in Table 8. We observe visually in Figure 11 that median filtering can physically remove scratch pixels from the image, while JPEG compression often fails to do so, which might explain median filtering’s effectiveness as a defense.

Method	ImageNet Recovery Rate	CIFAR-10 Recovery Rate
JPEG, q=85	0%	30.4%
JPEG, q=90	0%	36.58%
JPEG, q=95	0%	34.14%
JPEG, q=99	0%	24.3%
Median filter	100%	47.56%

Table 8: Recovery rate for ImageNet-trained ResNet-50 against double scratch Bézier curve attacks.

Certified Defenses. Furthermore, we evaluated the image-domain attack against certified defenses for adversarial patches [15], which provides a certificate of robustness, or an upper bound on the attack success rate for a given test set and L_0 -based threat model, which is most suited for our attack. We

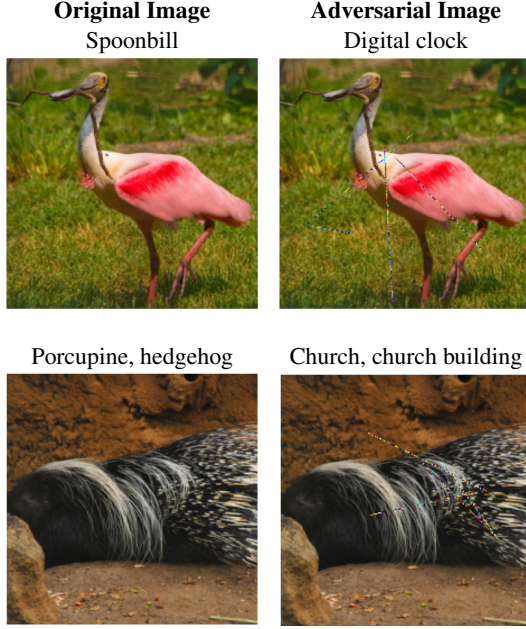


Figure 8: Examples of CMA-ES Bézier curves attacks in the network domain. Scratches were clipped to the image domain for visualization purposes. The left side shows the original images and their corresponding class; the right side shows the generated adversarial samples (scratches) and their respective predicted labels when evaluated on ResNet-50. Best viewed in color.

	plane	car	bird	cat	deer	dog	frog	horse	ship	truck	Row mean
plane	0	1879	1456	3003	3886	3144	2947	3478	3157	3039	2887
car	3407	0	4227	4631	6393	5560	3782	5370	3502	2462	4370
bird	889	2322	0	1587	1543	1043	1764	2324	4607	3929	2223
cat	2385	2505	1099	0	1820	1169	1835	2187	3677	2642	2146
deer	1267	1480	792	951	0	877	2007	1583	3183	2325	1607
dog	2465	2359	1760	677	2032	0	2384	2188	4605	3331	2422
frog	2100	2083	929	1151	2169	1619	0	3163	5568	3499	2475
horse	2319	2584	2655	1694	2942	1401	3659	0	5701	3051	2889
ship	704	1119	1776	2691	3574	2432	2070	3660	0	2145	2241
truck	2505	1400	4677	4579	5600	5421	5888	5033	4000	0	4344
Column mean	2004	1970	2152	2329	3328	2518	2926	3220	4222	2935	

Figure 9: Source-target dependency on CIFAR-10. Cell values correspond to the average number of queries to attack a source class (row) with a target class (column). The figure also shows the means of each row and column.

did not evaluate our attack against L_∞ or L_2 certified defenses as they lie outside our threat model. We trained a Convolutional Neural Network (CNN) from Chiang et al. [15] with four convolutional layers with kernel size (3, 4, 3, 4), stride (1, 2, 1, 2), output channels (4, 4, 8, 8), and two fully connected layers with 256 neurons on CIFAR-10. It achieved a test accuracy of 36.9% and a certified accuracy of 21.90% for L_0 attacks that lie within a 5×5 pixel patch.

	plane	car	bird	cat	deer	dog	frog	horse	ship	truck
plane	1.000	0.111	0.067	0.053	0.050	0.071	0.062	0.050	0.167	0.111
car	0.111	1.000	0.071	0.056	0.053	0.077	0.067	0.053	0.125	0.333
bird	0.067	0.071	1.000	0.143	0.125	0.167	0.250	0.125	0.071	0.071
cat	0.053	0.056	0.143	1.000	0.125	0.200	0.125	0.125	0.056	0.056
deer	0.050	0.053	0.125	0.125	1.000	0.125	0.111	0.143	0.053	0.053
dog	0.071	0.077	0.167	0.200	0.125	1.000	0.143	0.125	0.077	0.077
frog	0.062	0.067	0.250	0.125	0.111	0.143	1.000	0.111	0.067	0.067
horse	0.050	0.053	0.125	0.125	0.143	0.125	0.111	1.000	0.053	0.053
ship	0.167	0.125	0.071	0.056	0.053	0.077	0.067	0.053	1.000	0.125
truck	0.111	0.333	0.071	0.056	0.053	0.077	0.067	0.053	0.125	1.000

Figure 10: Similarity of CIFAR-10 classes computed with WordNet.

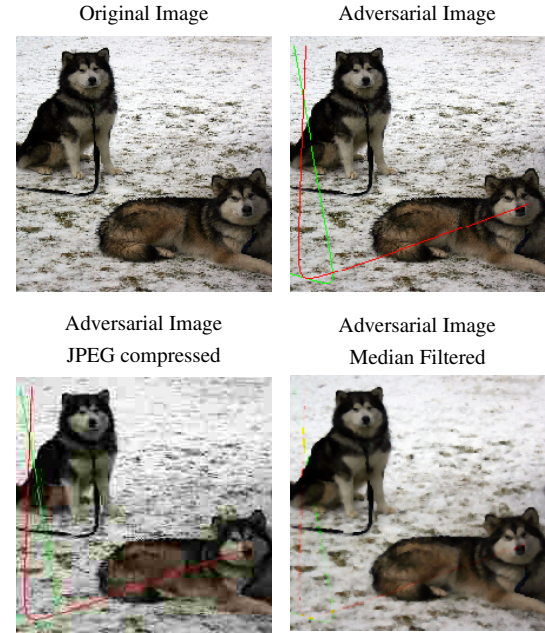


Figure 11: Best viewed in color. Filtering methods to counter adversarial noise. We visualize the results of various image compression mechanisms, namely JPEG compression and median filtering. JPEG compression fails to remove the scratches in an image, which might be responsible for its ineffectiveness as a defense. Median filtering on the other hand allows for much better smoothing and removal of the scratches.

Our attack on this network achieves a 2.2% success rate for 1000 CIFAR-10 images when taking into account the threat model of adversarial scratches falling within a 5×5 patch, and 34% when we remove this restriction. We find certified defenses to be a suitable defense against our attack. However, they are computationally intensive and currently cannot be scaled to larger neural networks such as those trained on ImageNet. Training certifiably robust neural networks for larger architectures remains an open problem.

6.4 Defenses in Network Domain

Here we discuss possible solutions to prevent the proposed attacks in the network domain. We evaluated the following techniques as defenses against adversarial scratched images:

- Clipping to the range [0, 1]; i.e., clip each pixel of the given image so that they fall into the image domain
- JPEG compression with varying quality factors
- Median filter applied to each channel separately with a kernel size of 3x3 pixels

To assess their performance, we use the notion of recovery rate defined in Section 6.3. Interestingly, we found out that about 21% of the attacks on CIFAR-10, even if we are in the network domain, fall in the image domain. All attacks on ImageNet fall outside the image domain. Tables 9 and 10 show the recovery rate with respect to all the available adversarial attacks. Table 9 also shows the recovery rate after splitting the attacks into the ones that are in the network domain and the ones that fall in the image domain to evaluate the performance of the defenses on each domain separately.

Method	Recovery Rate	Network Domain	Image Domain
Clipping	53%	70%	0%
JPEG, quality = 90	77%	86%	47%
JPEG, quality = 95	80%	90%	49%
JPEG, quality = 99	82%	91%	51%
Median filter	86%	88%	81%

Table 9: Performance of defense methods applied to network-domain fixed-location attacks on CIFAR-10. We highlight the recovery rates after performing image filtering on image domain scratches obtained from network domain attacks.

Method	Recovery Rate
Clipping	66%
JPEG, quality = 85	81%
JPEG, quality = 90	79%
JPEG, quality = 95	76%
JPEG, quality = 99	76%
Median filter	78%

Table 10: Performance of defense methods applied to network-domain fixed-location attacks on ImageNet.

Tables 11 and 12 show the performance impacts after applying the defense methods over the testset.

Considering both the effectiveness of the defense and the drop in model performance on benign images, JPEG compression appears to be the best defense in the network domain,

Method	Accuracy	Drop
No defense method	93.91%	—
Clipping	93.91%	0.00%
JPEG, quality = 99	93.72%	0.19%
Median filter	80.00%	13.91%

Table 11: Drop of ResNet-50 model performance after applying defense methods on CIFAR-10 testset.

Method	Accuracy	Drop
No defense method	76.13%	—
Clipping	76.13%	0.00%
JPEG, quality = 85	74.55%	1.58%
Median filter	71.97%	4.16%

Table 12: Drop of ResNet-50 model performance after applying defense methods on ImageNet testset.

due to its low impact on model performance and highest prevention rate, while median filtering appears to be the best defense for image domain attacks.

We can appreciate that the majority of image-domain attacks need fewer than 400 queries, corresponding to at most 10 iterations of the CMA-ES algorithm with a population size of 40, as described in Section 4.2.

7 Conclusion

In this paper, we proposed *adversarial scratches*, a new attack against neural networks inspired by the scratches that are commonly found in old printed photographs.

Our attack operates under strict assumptions: adversaries have access only to the predictions of a model (i.e, black-box access) and have limited ability in altering the input data. Our attack proved to be effective against not only several state-of-the-art deep neural network image classifiers, but also Microsoft’s Cognitive Services Image Captioning API. To offer a complete perspective, we also proposed mitigation strategies against our attack and demonstrated that we have the ability to restore the performance of the attacked models.

As future work, we aim to gain a better understanding of the correlation between source-target classes, their potential semantic similarities, and the success of the adversarial scratches attack. Furthermore, building upon the preliminary results obtained in this paper, we intend to expand our investigation on potential mitigation strategies. Additionally, we will expand our attack beyond the image classification. For instance, the equivalent of adversarial scratches for speech recognition systems can be posed as chirped sequences that appear benign, but might potentially be malicious.

References

- [1] Shadi Albarqouni, Christoph Baur, Felix Achilles, Vasileios Belagiannis, Stefanie Demirci, and Nassir Navab. Aggnet: Deep learning from crowds for mitosis detection in breast cancer histology images. *IEEE Transactions on Medical Imaging*, 35(5):1313–1321, 2016.
- [2] Moustafa Alzantot, Yash Sharma, Supriyo Chakraborty, and Mani Srivastava. GenAttack: Practical black-box attacks with gradient-free optimization. *arXiv preprint arXiv:1805.11090*, 2018.
- [3] Moustafa Alzantot, Yash Sharma, Ahmed Elgohary, Bo-Jhang Ho, Mani Srivastava, and Kai-Wei Chang. Generating natural language adversarial examples. *arXiv preprint arXiv:1804.07998*, 2018.
- [4] Anish Athalye, Nicholas Carlini, and David Wagner. Obfuscated gradients give a false sense of security: Circumventing defenses to adversarial examples. *arXiv preprint arXiv:1802.00420*, 2018.
- [5] Anish Athalye, Logan Engstrom, Andrew Ilyas, and Kevin Kwok. Synthesizing robust adversarial examples. *arXiv preprint arXiv:1707.07397*, 2017.
- [6] Trapit Bansal, Jakub Pachocki, Szymon Sidor, Ilya Sutskever, and Igor Mordatch. Emergent complexity via multi-agent competition. *arXiv preprint arXiv:1710.03748*, 2017.
- [7] Arjun Nitin Bhagoji, Warren He, Bo Li, and Dawn Song. Exploring the space of black-box attacks on deep neural networks. *arXiv preprint arXiv:1712.09491*, 2017.
- [8] Battista Biggio, Blaine Nelson, and Pavel Laskov. Poisoning attacks against support vector machines. *arXiv preprint arXiv:1206.6389*, 2012.
- [9] Tom B Brown, Dandelion Mané, Aurko Roy, Martín Abadi, and Justin Gilmer. Adversarial patch. *arXiv preprint arXiv:1712.09665*, 2017.
- [10] Nicholas Carlini and David Wagner. Adversarial examples are not easily detected: Bypassing ten detection methods. In *Proceedings of the 10th ACM Workshop on Artificial Intelligence and Security*, pages 3–14. ACM, 2017.
- [11] Nicholas Carlini and David Wagner. Towards evaluating the robustness of neural networks. In *2017 IEEE Symposium on Security and Privacy (SP)*, pages 39–57. IEEE, 2017.
- [12] Nicholas Carlini and David Wagner. Audio adversarial examples: Targeted attacks on speech-to-text. In *2018 IEEE Security and Privacy Workshops (SPW)*, pages 1–7. IEEE, 2018.
- [13] Pin-Yu Chen, Yash Sharma, Huan Zhang, Jinfeng Yi, and Cho-Jui Hsieh. EAD: elastic-net attacks to deep neural networks via adversarial examples. In *Thirty-second AAAI Conference on Artificial Intelligence*, 2018.
- [14] Pin-Yu Chen, Huan Zhang, Yash Sharma, Jinfeng Yi, and Cho-Jui Hsieh. Zoo: Zeroth order optimization based black-box attacks to deep neural networks without training substitute models. In *Proceedings of the 10th ACM Workshop on Artificial Intelligence and Security*, pages 15–26. ACM, 2017.
- [15] Ping-yeh Chiang, Renkun Ni, Ahmed Abdelkader, Chen Zhu, Christoph Studor, and Tom Goldstein. Certified defenses for adversarial patches. *arXiv preprint arXiv:2003.06693*, 2020.
- [16] Jacob Devlin, Ming-Wei Chang, Kenton Lee, and Kristina Toutanova. Bert: Pre-training of deep bidirectional transformers for language understanding. *arXiv preprint arXiv:1810.04805*, 2018.
- [17] Sergey Edunov, Myle Ott, Michael Auli, and David Grangier. Understanding back-translation at scale. *arXiv preprint arXiv:1808.09381*, 2018.
- [18] Gerald Farin, Josef Hoschek, and M-S Kim. *Handbook of computer aided geometric design*. Elsevier, 2002.
- [19] Ian J Goodfellow, Jonathon Shlens, and Christian Szegedy. Explaining and harnessing adversarial examples. *arXiv preprint arXiv:1412.6572*, 2014.
- [20] Chuan Guo, Jared S Frank, and Kilian Q Weinberger. Low frequency adversarial perturbation. *arXiv preprint arXiv:1809.08758*, 2018.
- [21] Chuan Guo, Jacob R Gardner, Yurong You, Andrew Gordon Wilson, and Kilian Q Weinberger. Simple black-box adversarial attacks. *arXiv preprint arXiv:1905.07121*, 2019.
- [22] Awni Hannun, Carl Case, Jared Casper, Bryan Catanzaro, Greg Diamos, Erich Elsen, Ryan Prenger, Sanjeev Satheesh, Shubho Sengupta, Adam Coates, et al. Deep speech: Scaling up end-to-end speech recognition. *arXiv preprint arXiv:1412.5567*, 2014.
- [23] Nikolaus Hansen. The CMA evolution strategy: A tutorial. *arXiv preprint arXiv:1604.00772*, 2016.
- [24] Kaiming He, Xiangyu Zhang, Shaoqing Ren, and Jian Sun. Deep residual learning for image recognition. In *Proceedings of the IEEE Conference on Computer Vision and Pattern Recognition*, pages 770–778, 2016.

- [25] Gao Huang, Zhuang Liu, Laurens Van Der Maaten, and Kilian Q Weinberger. Densely connected convolutional networks. In *Proceedings of the IEEE Conference on Computer Vision and Pattern Recognition*, pages 4700–4708, 2017.
- [26] Andrew Ilyas, Logan Engstrom, Anish Athalye, and Jessy Lin. Black-box adversarial attacks with limited queries and information. *arXiv preprint arXiv:1804.08598*, 2018.
- [27] Danny Karmon, Daniel Zoran, and Yoav Goldberg. Lavan: Localized and visible adversarial noise. *arXiv preprint arXiv:1801.02608*, 2018.
- [28] Alex Krizhevsky et al. Learning multiple layers of features from tiny images. Technical report, Citeseer, 2009.
- [29] Alex Krizhevsky, Ilya Sutskever, and Geoffrey E Hinton. Imagenet classification with deep convolutional neural networks. In *Advances in Neural Information Processing Systems*, pages 1097–1105, 2012.
- [30] Quan Le, Oisín Boydell, Brian Mac Namee, and Mark Scanlon. Deep learning at the shallow end: Malware classification for non-domain experts. *Digital Investigation*, 26:S118–S126, 2018.
- [31] Junyu Lin, Lei Xu, Yingqi Liu, and Xiangyu Zhang. Black-box adversarial sample generation based on differential evolution. *Journal of Systems and Software*, page 110767, 2020.
- [32] Aleksander Madry, Aleksandar Makelov, Ludwig Schmidt, Dimitris Tsipras, and Adrian Vladu. Towards deep learning models resistant to adversarial attacks. In *International Conference on Learning Representations*, 2018.
- [33] Microsoft. Cognitive Services Image Captioning API. <https://azure.microsoft.com/en-us/services/cognitive-services/computer-vision/>, 2020. [Online; accessed 18-June-2020].
- [34] George A Miller. Wordnet: a lexical database for english. *Communications of the ACM*, 38(11):39–41, 1995.
- [35] Apostolos Modas, Seyed-Mohsen Moosavi-Dezfooli, and Pascal Frossard. Sparsefool: a few pixels make a big difference. In *Proceedings of the IEEE Conference on Computer Vision and Pattern Recognition*, pages 9087–9096, 2019.
- [36] Seyed-Mohsen Moosavi-Dezfooli, Alhussein Fawzi, and Pascal Frossard. DeepFool: a simple and accurate method to fool deep neural networks. In *Proceedings of the IEEE Conference on Computer Vision and Pattern Recognition*, pages 2574–2582, 2016.
- [37] Nina Narodytska and Shiva Kasiviswanathan. Simple black-box adversarial attacks on deep neural networks. In *2017 IEEE Conference on Computer Vision and Pattern Recognition Workshops (CVPRW)*, pages 1310–1318. IEEE, 2017.
- [38] Nicolas Papernot, Patrick McDaniel, Somesh Jha, Matt Fredrikson, Z Berkay Celik, and Ananthram Swami. The limitations of deep learning in adversarial settings. In *2016 IEEE European Symposium on Security and Privacy (EuroS&P)*, pages 372–387. IEEE, 2016.
- [39] Alec Radford, Jeffrey Wu, Rewon Child, David Luan, Dario Amodei, and Ilya Sutskever. Language models are unsupervised multitask learners. *OpenAI Blog*, 1(8):9, 2019.
- [40] Edward Raff, Jon Barker, Jared Sylvester, Robert Brandon, Bryan Catanzaro, and Charles K Nicholas. Malware detection by eating a whole exe. In *Workshops at the Thirty-Second AAAI Conference on Artificial Intelligence*, 2018.
- [41] Yash Sharma and Pin-Yu Chen. Attacking the madry defense model with l_1 -based adversarial examples. *arXiv preprint arXiv:1710.10733*, 2017.
- [42] Wei Shen, Mu Zhou, Feng Yang, Caiyun Yang, and Jie Tian. Multi-scale convolutional neural networks for lung nodule classification. In *International Conference on Information Processing in Medical Imaging*, pages 588–599. Springer, 2015.
- [43] Ilia Shumailov, Yiren Zhao, Daniel Bates, Nicholas Papernot, Robert Mullins, and Ross Anderson. Sponge examples: Energy-latency attacks on neural networks. *arXiv preprint arXiv:2006.03463*, 2020.
- [44] David Silver, Aja Huang, Chris J Maddison, Arthur Guez, Laurent Sifre, George Van Den Driessche, Julian Schrittwieser, Ioannis Antonoglou, Veda Panneershelvam, Marc Lanctot, et al. Mastering the game of go with deep neural networks and tree search. *Nature*, 529(7587):484, 2016.
- [45] David Silver, Thomas Hubert, Julian Schrittwieser, Ioannis Antonoglou, Matthew Lai, Arthur Guez, Marc Lanctot, Laurent Sifre, Dharshan Kumaran, Thore Graepel, et al. Mastering chess and shogi by self-play with a general reinforcement learning algorithm. *arXiv preprint arXiv:1712.01815*, 2017.
- [46] Karen Simonyan and Andrew Zisserman. Very deep convolutional networks for large-scale image recognition. *arXiv preprint arXiv:1409.1556*, 2014.

- [47] Jiawei Su, Danilo Vasconcellos Vargas, and Kouichi Sakurai. One pixel attack for fooling deep neural networks. *IEEE Transactions on Evolutionary Computation*, 2019.
- [48] Christian Szegedy, Vincent Vanhoucke, Sergey Ioffe, Jon Shlens, and Zbigniew Wojna. Rethinking the inception architecture for computer vision. In *Proceedings of the IEEE Conference on Computer Vision and Pattern Recognition*, pages 2818–2826, 2016.
- [49] Christian Szegedy, Wojciech Zaremba, Ilya Sutskever, Joan Bruna, Dumitru Erhan, Ian Goodfellow, and Rob Fergus. Intriguing properties of neural networks. *arXiv preprint arXiv:1312.6199*, 2013.
- [50] R Vinayakumar, Mamoun Alazab, KP Soman, Prabaharan Poornachandran, and Sitalakshmi Venkatraman. Robust intelligent malware detection using deep learning. *IEEE Access*, 7:46717–46738, 2019.
- [51] Oriol Vinyals, Igor Babuschkin, Wojciech M Czarnecki, Michaël Mathieu, Andrew Dudzik, Junyoung Chung, David H Choi, Richard Powell, Timo Ewalds, Petko Georgiev, et al. Grandmaster level in StarCraft II using multi-agent reinforcement learning. *Nature*, pages 1–5, 2019.
- [52] Chenglin Yang, Adam Kortylewski, Cihang Xie, Yinzhi Cao, and Alan Yuille. Patchattack: A black-box texture-based attack with reinforcement learning. *arXiv preprint arXiv:2004.05682*, 2020.
- [53] Alois Zingl. A rasterizing algorithm for drawing curves. 2012.